Article

New Water-Ethylene Glycol Lubricants with Stearate Ionic Liquid Crystal Additive

María-Dolores Avilés [1], Cristian Sánchez-Rodríguez [1,2], Ramón Pamies [1], María-Dolores Bermúdez [1,*], Francisco-José Carrión-Vilches [1], Susana García Sanfelix [2] and Anna-Lena Kjøniksen [2]

1   Grupo de Ciencia de Materiales e Ingeniería Metalúrgica, Universidad Politécnica de Cartagena, Campus de la Muralla del Mar, 30202 Cartagena, Spain
2   Faculty of Engineering, Østfold University College, P.O. Box 700, 1757 Halden, Norway
*   Correspondence: mdolores.bermudez@upct.es

Abstract: The main purpose of the present study is to improve the tribological performance of aqueous lubricants with the use of ecofriendly, fatty acid-derived additives. The protic ionic liquid crystal bis(2-hydroxyethyl)ammonium stearate (DES) has been added to 50:50 water+ethylene glycol (W–EG) to obtain (W–EG)+0.5%DES; (W–EG)+1%DES and (W–EG)+2%DES emulsions. The new lubricants have been studied in sapphire-AISI (American Iron and Steel Institute) 316L stainless-steel pin-on-disk sliding contacts. The addition of DES reduces the friction coefficient by up to 76% and wear rate by up to 80%, with respect to (W–EG). The best performance is found for the emulsions with the lower proportion of DES (0.5 and 1 wt.%). These results have been related to viscosity and turbidity values. Wear mechanisms have been studied by Scanning Electron Microscopy/Energy Dispersive X-ray Spectroscopy (SEM/EDX) and by Raman microscopy. While W–EG shows a severe abrasive mechanism, no abrasion marks are present inside the wear track after lubrication with (W–EG)+0.5%DES, the emulsion with the lowest wear rate. After lubrication with W–EG, an increase in oxygen content is observed inside the wear track, as determined by EDX and confirmed by Raman microscopy, which shows the presence of iron oxides. The addition of DES reduces these oxidation processes.

Keywords: water; ethylene glycol; protic ionic liquid

1. Introduction

Fluids containing glycols find a wide range of applications mainly due to their thermal properties. In tribological applications, they are used both as base fluids and as friction-reducing additives in aqueous lubrication [1].

Water-ethylene glycol solutions are stable fluids with higher boiling temperatures, lower freezing points than water. These characteristics, together with the reduction in the severe corrosion caused by water, have raised interest in the improvement of the tribological performance of different water–glycol systems [2–4] and, in particular, of water-ethylene glycol [5–9].

Ionic liquids have received much attention as lubricants [10] and lubricant additives [11]. With the increasing need for eco-friendly and biodegradable lubricants, mineral-base oils are substituted with synthetic oils and aqueous lubricants. In the same way, conventional ionic liquids composed of heterocyclic cations and halogenated anions are being replaced by less-toxic and less-corrosive compositions containing alkyl phosphonium and ammonium cations combined with halogen-free anions.

Protic ionic liquids (PILs) [12] with carboxylate anions and protic ammonium cations are ionic liquids with minor or non-toxic effects and high biodegradability [13]. The simplicity of their synthetic route [14] has also contributed to the expansion of the number of studies focused on them.

One of the present priorities in tribology is the development of new aqueous lubricants with improved performance [15–21]. PILs have already shown promising results as additives in water. Solutions of short alkyl chain protic ammonium carboxylate PILs in water reach ultralow friction [20,21], but only after water evaporation has taken place at the sliding contact. Long alkyl chain PILs such as those derived from fatty acids [22–28] are not soluble in water, but they form emulsions that are able to provide strong friction and wear reductions. Although these fatty acid-derived PILs increase thermal stability and delay water evaporation to longer sliding distances, they are not able to completely prevent it, at least when used as 1 wt.% additives. Hence, there is a need for more thermally stable aqueous base lubricants. In a previous work [28] we have used a short alkyl chain PIL as base fluid and a long alkyl chain PIL as additive with excellent results. Water-glycol fluids are also a suitable alternative to pure water, with a low cost and a wide range of applications.

Recent studies have focused on the use of ionic liquids in water-glycol systems [7–9,25,26,29,30], but the use of ionic liquid as friction-reducing and antiwear additives in water-ethylene glycol base lubricants has very limited precedent. Most recent studies [25] have shown the good tribological performance of the water-ethylene glycol-protic ionic liquid system. In the same vein, Zheng et al. [26] have shown the ability of ammonium carboxylate PILs and, in particular, of a ricinoleic acid derivative to improve the lubricating performance of 50:50 water-ethylene glycol in steel-steel contact under reciprocating sliding conditions. However, the ionic liquids used in that study contained a N,N-dimethylethanolamine monoprotic cation, and only one composition (0.5 wt.%) was studied, in a metal-metal contact, rather than in a ceramic-metal contact as in the present case.

In the present study, new emulsions have been obtained from 50:50 water-ethylene glycol by addition of bis(2-hydroxyethyl)ammonium stearate (DES), one of the fatty acid derived PILs previously studied as additives in water [27], and in a short chain ammonium carboxylate PIL [28].

2. Materials and Methods

The protic ionic liquid crystal bis(2-hydroxyethyl)ammonium stearate (DES) (see chemical formula in Figure S1 in Supplementary Materials) used in the present work has been previously described [14] and was added in different concentrations (0.5 wt.%, 1 wt.% and 2wt.%) to a solution of ethylene glycol, $HO(CH_2)_2OH$ (EG) (Panreac, 99%) and deionized water at a 50:50 mass ratio. The new lubricant blends were ultrasonicated for 30 min at 30 °C.

A DSA 30B (Krüss, Hamburg, Germany) analyzer was used to measure the contact angles on the AISI 316L surface. Raman microscopy spectra were recorded using a Witec UHTS 300 (WITec GmbH, Ulm, Germany) spectrometer and a 532 nm laser, respectively. A TGA 1HT (Mettler Toledo, Columbus, OH, USA) was used for thermogravimetric analysis (TGA) at a 5 °C/min heating rate, under N_2 atmosphere (50 mL/min) in the temperature range from room temperature to 500 °C.

Friction values of sapphire balls (Goodfellow, London, UK) [Al_2O_3; 99.9%; HV 2750; Young's modulus 445 GPa; Poisson's ratio 0.24] against AISI 316L stainless steel disks of 25 mm diameter [HV 200; Young's modulus 197 GPa; Poisson's ratio 0.27] were recorded by a pin-on-disk tribometer (TRB Anton Paar, Zürich, Switzerland) under ambient conditions (26.4 ± 0.2 °C; 67.4 ± 1.3%HR). Stainless steel disks were previously polished using a vibratory polishing device Saphir Vibro (QATM, Mammelzen, Germany) for 90 min at a frequency of 85 Hz, to obtain an average roughness (*Ra*) <26 nm. To ensure reproducibility, the tribological tests were repeated at least three times under a normal load of 1N (mean contact pressure 1.30 GPa; maximum contact pressure 1.95 GPa), with a sliding radius of 5.0 mm, a speed of 0.063 m/s, a sliding distance of 1000 m and a lubricant volume of 0.2 mL After each tribological test, disks were cleaned with distilled water and dried with hot air. Wear rates were calculated from cross section areas of the wear tracks (see Figure S2 in Supplementary Materials) and wear track length, as: [(A2 − (A1 + A3)) × (wear track

length)]. At least three tests were conducted for each set of experimental conditions in order to calculate average values and deviations.

Roughness, surface topography and wear measurements of AISI 316L disks were determined by means of a Talysurf CLI 500 (Taylor Hobson, Leicester, UK) optical profilometer. A scanning electron microscope (SEM) S3500 N (Hitachi, Tokyo, Japan) was used to obtain electron micrographs and energy dispersive X-ray (EDX) spectra of the wear tracks.

Viscosity measurements were made using a double plate rheometer (AR-G2; TA Instruments, Lubbock, TX, USA), with a Peltier temperature control system. The effect of temperature on the viscosity of the dispersions and solvent was recorded at a constant shear rate of 50 s^{-1} from 25 to 100 °C with an increase of 10 °C/min.

The temperature dependence of the turbidity of the lubricant fluids was investigated using a spectrophotometer (Thermo Scientific UV-VIS Evolution 201, Fisher Scientific, Hampton, NH, USA) at a wavelength of 500 nm. The transmittance was measured within the temperature range of 20–55 °C at a heating rate of 1 °C/min. The turbidity (τ) was determined by Equation (1):

$$\tau = -\frac{1}{L}ln\frac{I_t}{I_o} \tag{1}$$

where L is the path length of the cuvette (1 mm), and I_t and I_o are the transmitted light intensity through the sample and through water, respectively.

In order to study how the turbidity was influenced by shear forces, experiments were carried out at different shear rates using an Anton Paar MCR302 (Anton Paar, Graz, Australia) with a plate-plate measuring system mounted in a cylindrical Peltier system for temperature control. The measurements were conducted utilizing a gap of 0.5 mm in steady state. Temperature ramps were conducted at a constant shear rate of 50 s^{-1} under a heating velocity of 1 °C/min, from 20 to 55 °C.

3. Results and Discussion

Figure 1 shows thermogravimetric analysis results for all fluids, neat water (W), ethylene glycol (EG), the protic ionic liquid crystal DES and the four lubricants. It can be observed that the thermal stability of the emulsions containing the protic ionic liquid crystal DES are similar to that of the water-ethylene glycol solution (W–EG), with onset temperature at 99 °C. The 50% weight loss temperature of 137.7 °C for W–EG, increases with increasing DES content, to 141.2 °C for (W–EG) + 0.5%DES, 145.2 °C for (W–EG) + 1%DES and 148.2 °C for (W–EG) + 2%DES.
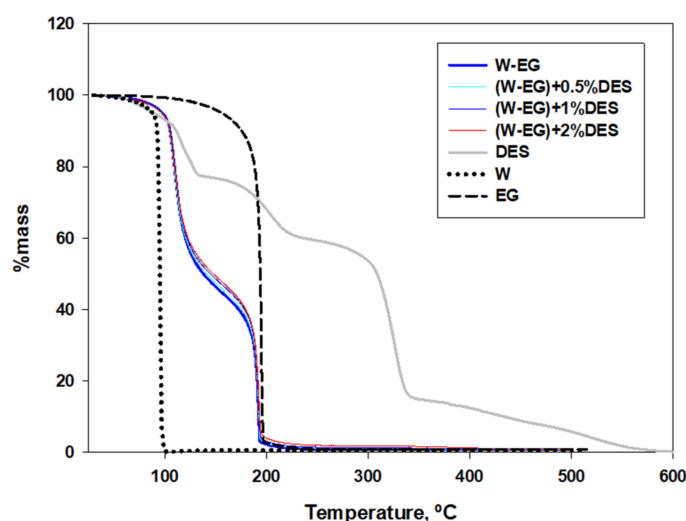

Figure 1. Thermogravimetric analysis curves for all fluids.

Raman spectra of the emulsions (Figure 2) are similar to that of the W–EG solution, without changes due to the addition of DES, in the low proportion used in the present study.
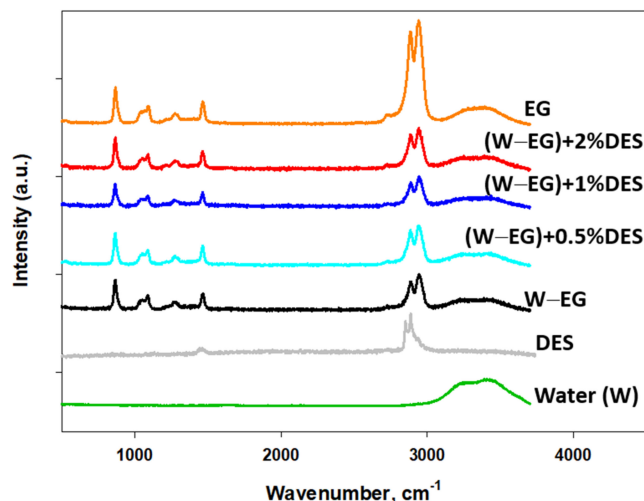

Figure 2. Raman spectra of all fluids.

Water (W) shows the characteristic broad bands between 3200 and 3500 cm^{-1}. These bands are also present, with a lower intensity, in all lubricants containing water and in ethylene glycol (EG), as they are characteristic of the –OH stretching vibrations.

EG [31] also shows intense bands between 2700 and 2950 cm^{-1}, assignable to C-H stretching. A weak band at 1466.5 cm^{-1} corresponds to CH$_2$ bending, while weak peaks at 1094.5 and 868.8 cm^{-1} are assigned to C-O and C-C stretching, respectively.

Figure 3a shows that 50:50 water-ethylene glycol (W–EG) is a transparent solution. Although DES is not completely soluble in W–EG, the emulsions containing 0.5; 1 or 2 wt.% DES (Figure 3b–d) are stable and no sedimentation occurred after at least 30 days at room temperature.
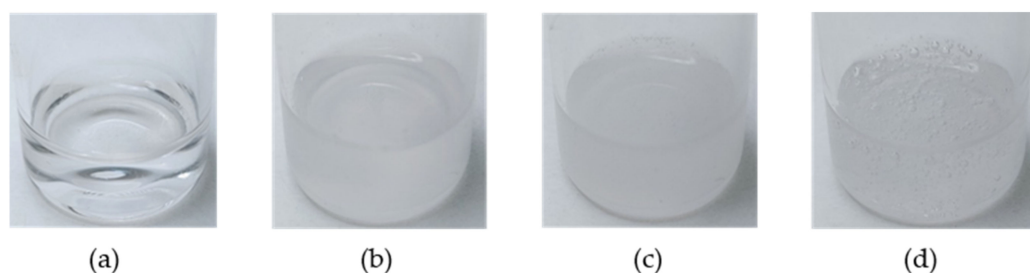

Figure 3. Photographs of the lubricants at room temperature: (**a**) W–EG; (**b**) (W–EG) + 0.5%DES; (**c**) (W–EG) + 1%DES; (**d**) (W–EG) + 2%DES.

As seen in Figure 4, the evolution of turbidity results with temperature for W–EG and the emulsions has also been studied.

As expected, turbidity values (Figure 4 and Table 1) increase as the concentration of the ionic liquid crystal additive (DES) increases. In the cases of (W–EG) + 0.5%DES and (W–EG) + 1%DES, turbidity values show a mild decrease for temperatures in the range between 40 °C and 50 °C, in agreement with the transition to the ordered mesomorphic structure of the ionic liquid crystal [32,33]. When the critical temperature of 50 °C is reached (Figure 4 and Table 1), a sharp decrease in turbidity is observed for (W–EG) + 2%DES, because of the contraction of the aggregates. A new increase in turbidity is observed at high temperatures, to recover the initial order of turbidity values. The relative instability of (W–EG) + 2%DES could anticipate a poorer tribological performance.
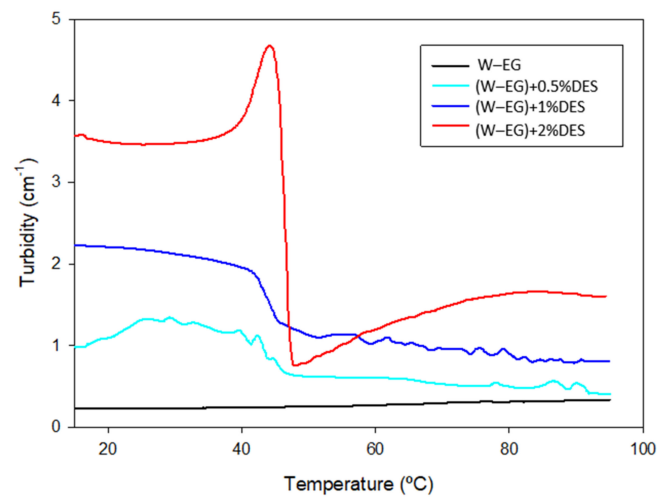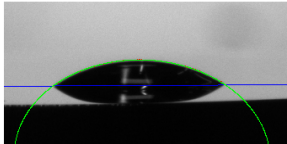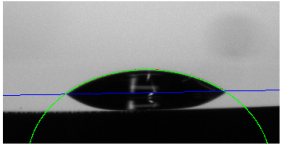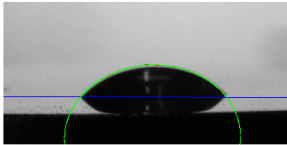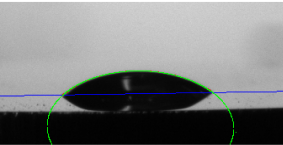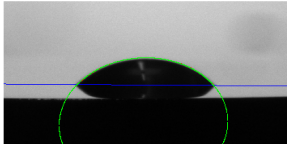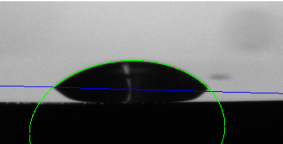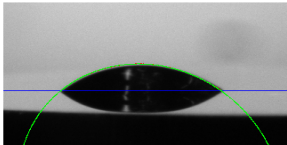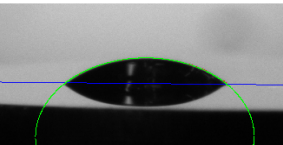
Figure 4. Temperature effect on the turbidity of the dispersions.

Table 1. Turbidity values for the four lubricants at different temperatures.

Lubricant	Turbidity (cm^{-1})				
	15 °C	**40 °C**	**44 °C**	**50 °C**	**95 °C**
W–EG	0.23	0.25	0.25	0.24	0.34
(W–EG) + 0.5%DES	0.97	1.60	0.76	0.62	0.39
(W–EG) + 1%DES	2.22	1.96	1.54	1.12	0.90
(W–EG) + 2%DES	3.57	3.77	4.68	0.80	1.60

Table 2 shows the increase in the instantaneous contact angle of W–EG on AISI 316L stainless steel with the addition of DES. The highest increase in the initial contact angle is observed for the lowest DES concentration, and is reduced with further DES addition.

Table 2. Contact angles for all lubricants on AISI 316L steel surface.

Lubricant	Initial	After 5 min
W–EG	 35.6° (2.1)	 33.8° (1.6)
(W–EG) + 0.5%DES	 53.1° (3.9)	 41.9° (2.0)
(W–EG) + 1%DES	 51.1° (5.0)	 49.0° (4.7)
(W–EG) + 2%DES	 46.4° (4.4)	 41.2° (1.5)

After a period of 5 min, once steel-surface interactions with the polar molecules and ions present in the fluids have taken place, contact angles are reduced for all lubricants, the highest decrease being observed for (W–EG) + 0.5% DES. These results are in agreement with contact angle increase recently described by Su et al. [25] for PILs in water-ethylene glycol. The reduction in the wettability of W–EG is attributed to the preferential interaction between DES molecules and the stainless steel surface.

The results of the rheological studies (Figures 5 and 6) show that W–EG solution is a Newtonian fluid with a low viscosity value of 3 mPa·s, three times higher than that of water.
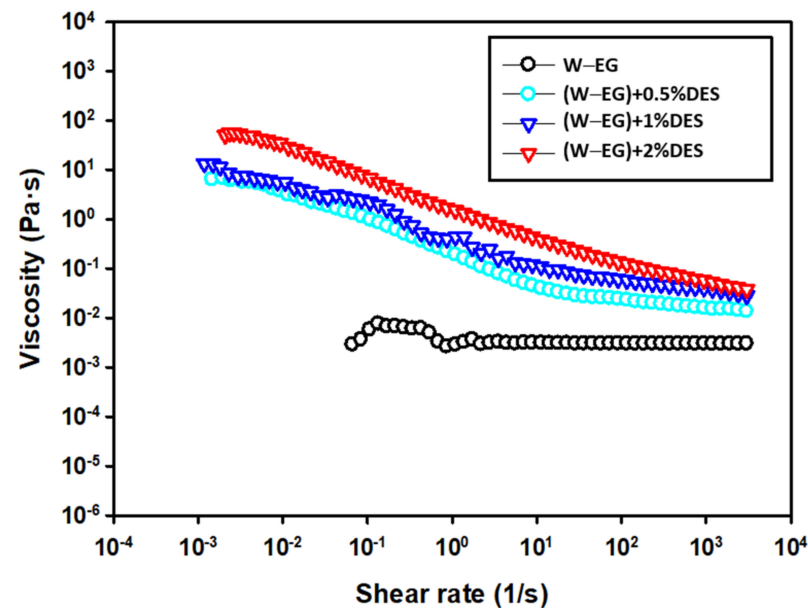
Figure 5. Effect of shear rate on the viscosity of the lubricants.
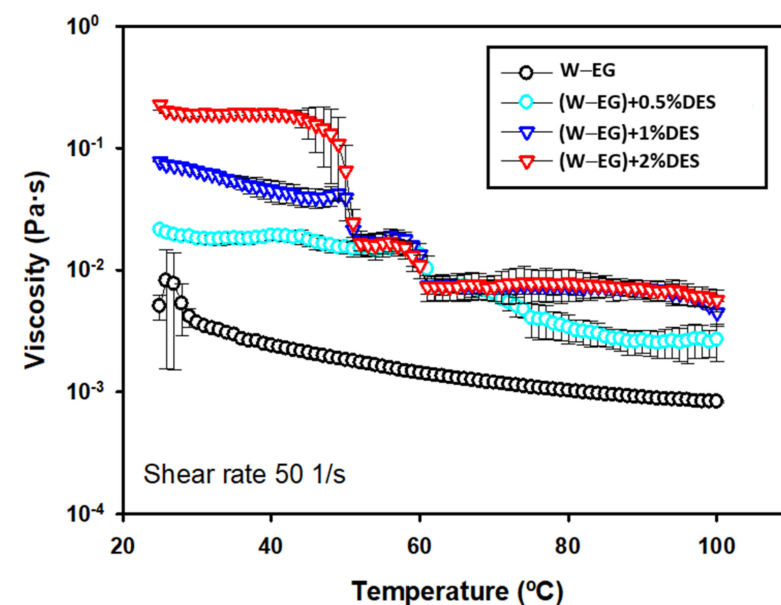
Figure 6. Effect of temperature on the viscosity of the lubricants.

Figure 5 shows that the addition of DES to the W–EG solution leads to emulsions with much higher viscosity. As expected, viscosity values increase with increasing DES concentration. At low shear rates, the viscosity is increased by several orders of magnitude. This could be ascribed to the presence of large agglomerates of DES. The emulsions show a

strong thinning effect when the shear rate is increased, probably due to the disruption of the agglomerates at high stress [24].

In Figure 6, the effect of temperature on the viscosity of all fluids is observed. The data were recorded at a constant shear rate of 50 s^{-1} from 25 to 100 °C with an increase of 10 °C/min. The W–EG solution shows a smooth decrease in viscosity with increasing temperature values. Conversely, the (W–EG) + DES emulsions show steep transitions to lower viscosity values at 50 and 60 °C, which are more pronounced as the concentration of DES increases. This is a typical behavior of ionic liquid crystals with different molecular ordering at different temperatures [32]. In a previous work, a mesomorphic transition of pure DES was determined at 53.3 °C [22]. The abrupt decrease in the viscosity could be assigned to the contraction of the agglomerates. When the mesomorphic transition of DES is reached, a contraction of the structures could occur because of the higher ordering and compaction of the new phase. At the highest concentration of 2 wt. % and at high temperatures (over 70 °C) an increase in the size would take place. When the temperature is raised, a weakening of the interaction of DES with the solvent could occur, and the hydrophobicity of the ionic liquid crystal is increased. Therefore, the formation of larger aggregates by associations of DES molecules is promoted [34].

Tribological Results

Neat water lubrication produces very high friction coefficients [1,20,26]. Table 3 shows average coefficients of friction and wear rates for all lubricants. We have previously studied [26] the effect of the addition of 1 wt.% DES to water. A reduction in the friction coefficient from 0.38 for neat water to 0.11 for water + 1%DES was achieved.

Table 3. Coefficients of friction (*COF*) and wear rates values.

Lubricant	*COF*	Wear Rate (mm³/N·m)
W–EG	0.28 (±0.019)	1.92×10^{-5} (±1.47×10^{-6})
(W–EG) + 0.5%DES	0.08 (±0.004)	4.01×10^{-6} (±2.22×10^{-7})
(W–EG) + 1%DES	0.07 (±0.007)	6.40×10^{-6} (±5.80×10^{-7})
(W–EG) + 2%DES	0.09 (±0.009)	1.06×10^{-5} (±5.32×10^{-7})

The high thermal stability of the water+ethylene glycol solution avoids evaporation, but it is also a poor lubricant, as the friction coefficient and wear rate are still very high. A mean friction coefficient of 0.28 is obtained (Table 3). The new emulsions containing the ionic liquid crystal DES show outstanding tribological performance. The higher friction reductions of 72% and 76% are obtained for the emulsion containing 0.5 and 1wt% DES, respectively.

Figure 7 shows the variation in the coefficient of friction with sliding distance for all lubricant blends. W–EG is not an efficient lubricant, showing high friction values, with severe stick-slip. All emulsions present extraordinary friction-reduction ability with respect to W-EG, with coefficients of friction lower than 0.1 in all cases.

Figure 8 allows for a more detailed analysis of the evolution of friction coefficients with sliding distance for the three DES-containing emulsions. The lowest initial friction values are obtained for the emulsion containing 1 wt.%DES. While (W–EG) + 2%DES increases friction with sliding distance, friction coefficients for (W–EG) + 0.5%DES and (W–EG) + 1%DES are kept constant for the first 350 m of sliding distance. From this point, both emulsions show opposite evolutions, with decreasing friction for (W–EG) + 0.5%DES, while friction increases for (W–EG) + 1%DES. In this way, friction curves meet for both emulsions from 500 m, once a steady-state lubrication regime has been established, to the

end of the tests, after 1000 m. These results could be related to viscosity and turbidity values for these emulsions.
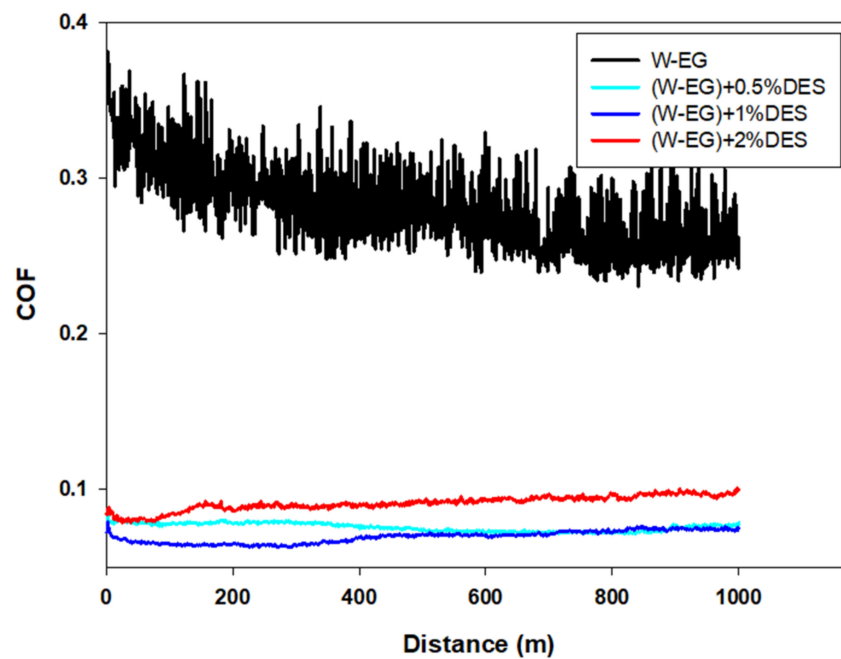

Figure 7. Variation in coefficients of friction (*COF*) with sliding distance for all lubricants.
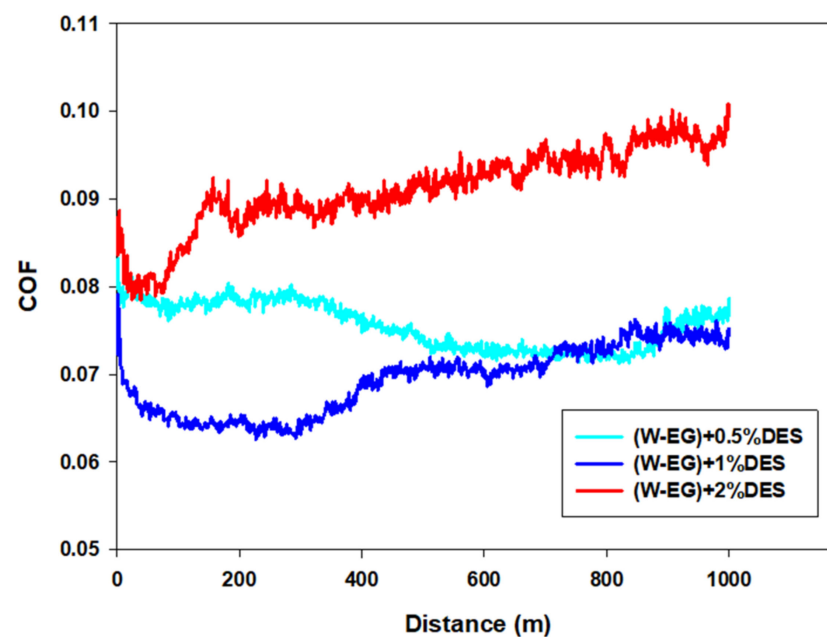
Figure 8. Variation in the coefficient of friction (*COF*) with sliding distance for the three (W–EG) + DES emulsions.

Figure 9 and Table 3 show wear rate values for all lubricants. W–EG shows severe wear in agreement with the high friction value. The best antiwear performance is found for (W–EG) + 0.5%DES, with 80% reduction with respect to water + ethyleneglycol. (W–EG) + 1%DES also shows a very good antiwear ability with 77% wear rate reduction.
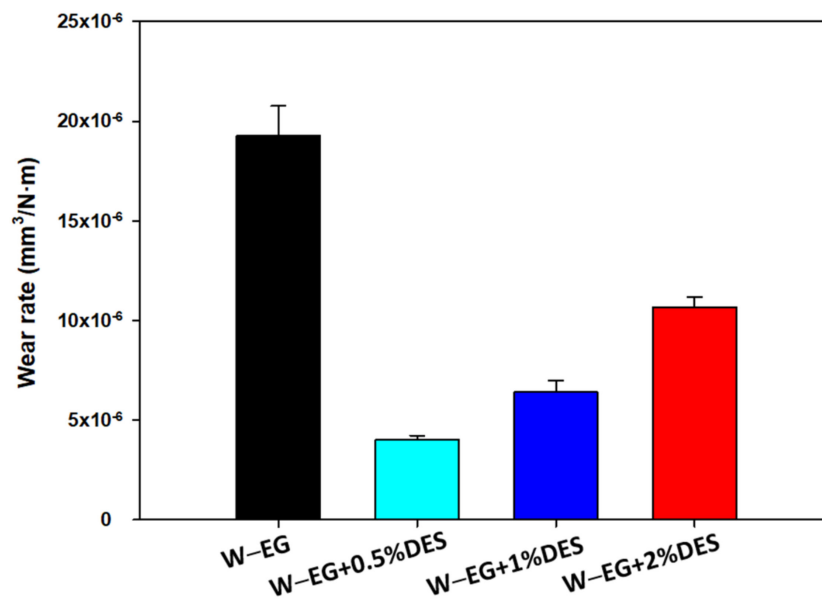
Figure 9. Wear rates of AISI 316L disks for each lubricant.

The severity of the contact conditions under W–EG lubrication can be observed, not only by the high friction coefficient and high wear rate for the stainless steel disk, but also by the surface damage produced on the pin sliding material, in this case a sapphire ball. The surface topography of the sapphire ball after lubrication with W–EG shows the presence of a wear scar on the spherical end, which has been in contact with the steel surface during sliding (Figure 10).
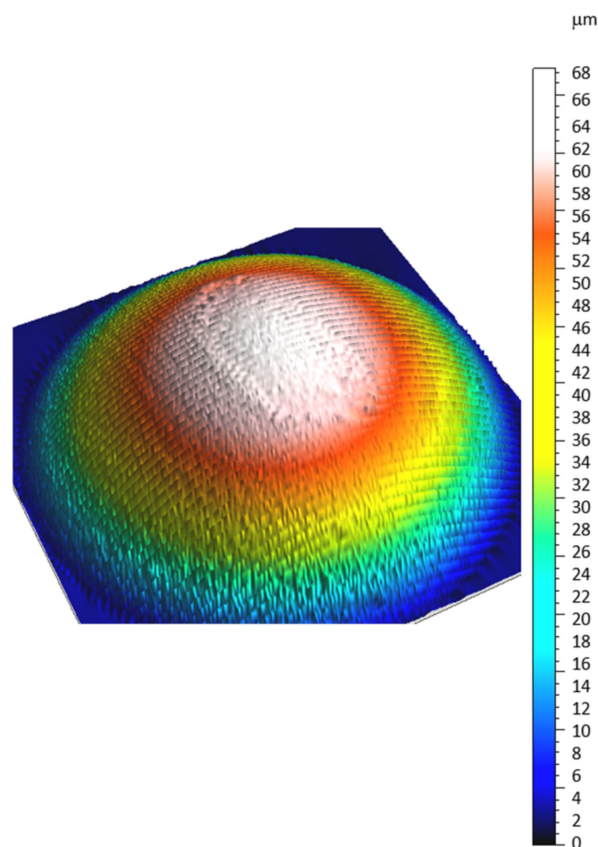

Figure 10. Profilometry image of the wear scar on sapphire ball after lubrication with W–EG.

The surface of the wear track on the steel disk after lubrication with W–EG (Figure 11a,b) shows a severe plastic deformation, with material accumulation over the edges (as pointed to by the arrow) and a very pronounced stick-slip effect, as seen by the periodical changes in wear track width (Figure 11a). Moreover, the magnification image in Figure 11b, shows the presence of deep abrasion marks (as pointed to by the arrow), parallel to sliding direction.
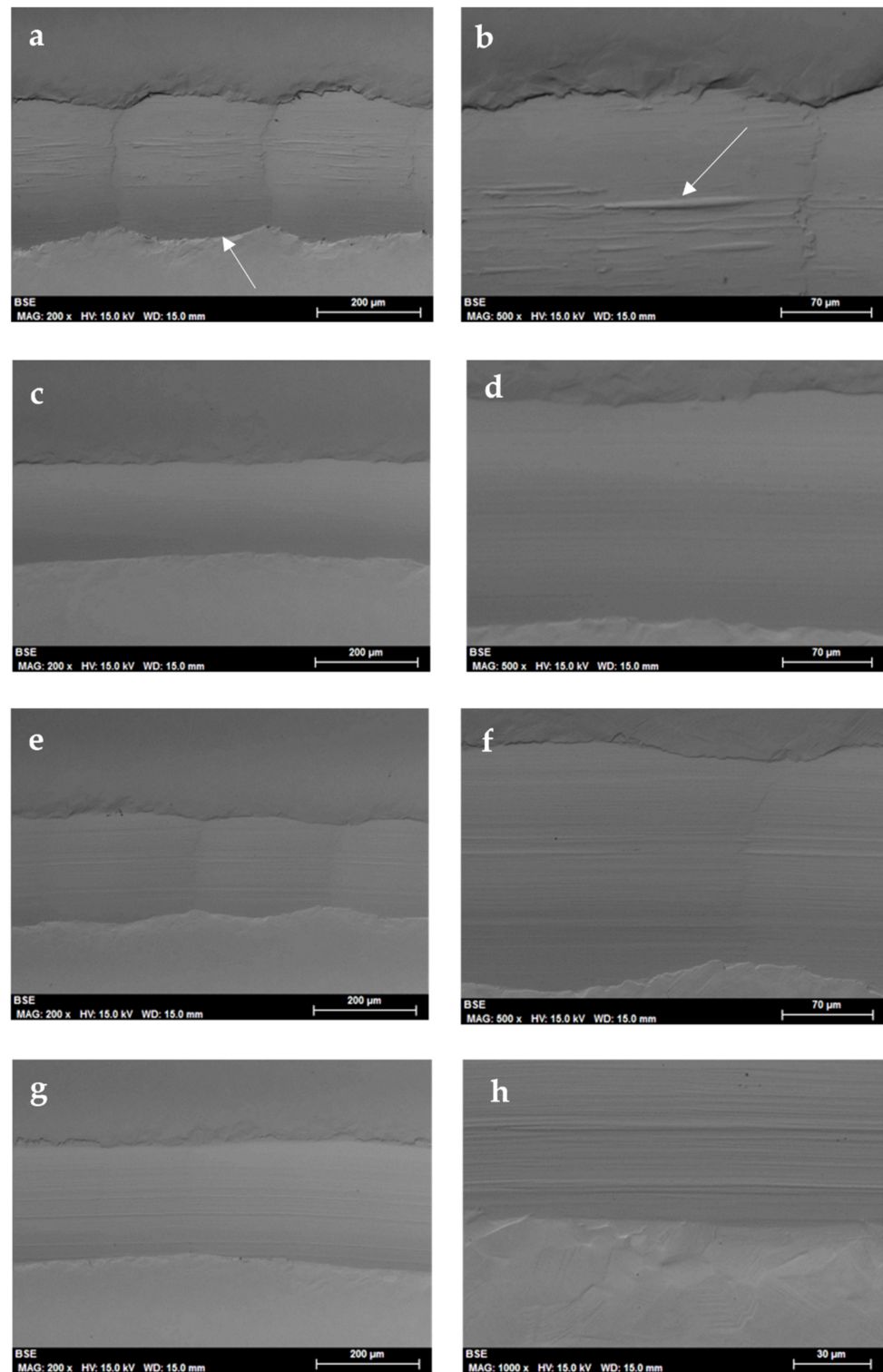
Figure 11. SEM micrographs of the wear scars on the steel disks after lubrication with W–EG (**a,b**); (W–EG) + 0.5%DES (**c,d**); (W–EG) + 1%DES (**e,f**); (W–EG) + 2%DES (**g,h**).

For (W–EG) + 0.5%DES, a smooth, narrow wear path is observed (Figure 11c,d), without the presence of abrasion grooves.

The abrasive mechanism is observed again for (W–EG) + 1%DES, with mild abrasion marks inside the wear track (Figure 11e,f), and its severity increases further in the case of (W–EG) + 2%DES (Figure 11g,h).

EDX spectra of the wear tracks are similar for all lubricants. Figure 12 shows a typical EDX spectrum of a wear track, showing the characteristics elements present in AISI 316L stainless steel.
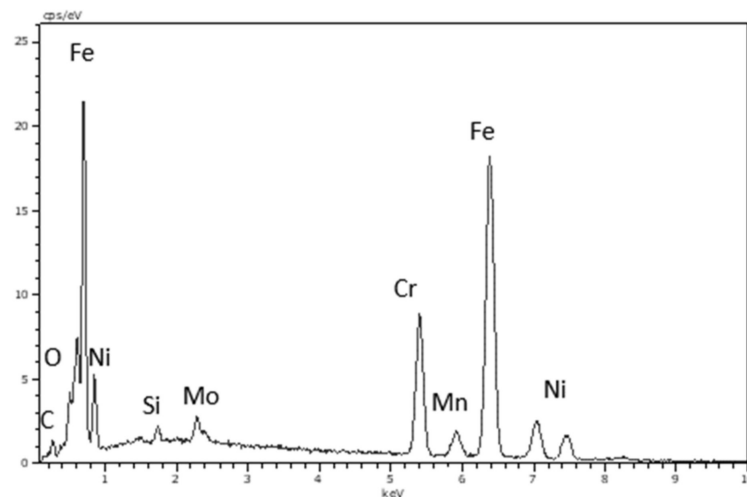

Figure 12. EDX spectrum of the wear tracks on AISI 316L steel disks.

Table 4 shows the chemical composition obtained by EDX inside and outside the wear tracks after lubrication tests. For W–EG, a reduction in iron and chromium percentages inside the wear track is observed, together with an increase in carbon and, especially, a strong increment in oxygen concentration, which is multiplied by a factor of 3.5 inside the wear track, with respect to the oxygen content outside the worn area.

Table 4. EDX element percentages inside and outside the wear tracks after lubrication.

Lubricant	Element (wt.%)							
	Fe		C		O		Cr	
	Inside	Outside	Inside	Outside	Inside	Outside	Inside	Outside
W–EG	56.9	61.2	10.4	7.3	7.6	2.2	13.9	15.4
(W–EG) + 0.5%DES	59.7	62.0	8.7	7.8	3.3	1.4	15.1	15.6
(W–EG) + 1%DES	60.9	61.6	7.5	7.7	2.8	1.7	15.4	15.5
(W–EG) + 2%DES	60.4	61.1	9.1	7.9	1.8	1.6	15.1	15.5

In contrast, when the emulsions of DES in W–EG are used as lubricants, the composition of the worn areas are very similar to that of the original surface of the stainless steel disk.

The increase in oxygen content observed by EDX analysis after lubrication with W-EG indicates that oxidation processes have taken place. Raman microscopy has been used in order to study the nature of these processes.

Figure 13 shows the Raman spectrum corresponding to the selected point at the center of the wear track after lubrication with W–EG. The more intense bands at 218.8 and 270.4 cm^{-1} are assignable to iron oxide, Fe_2O_3 [35,36].
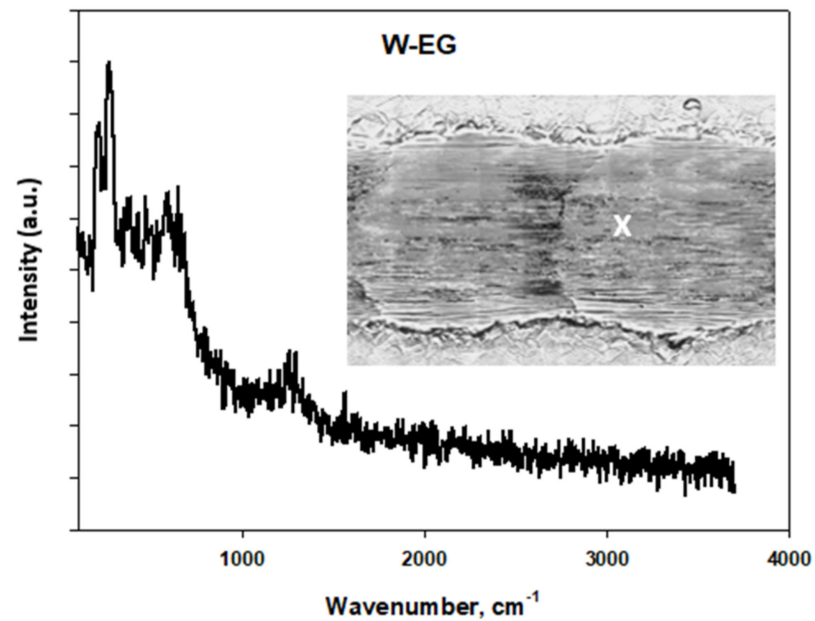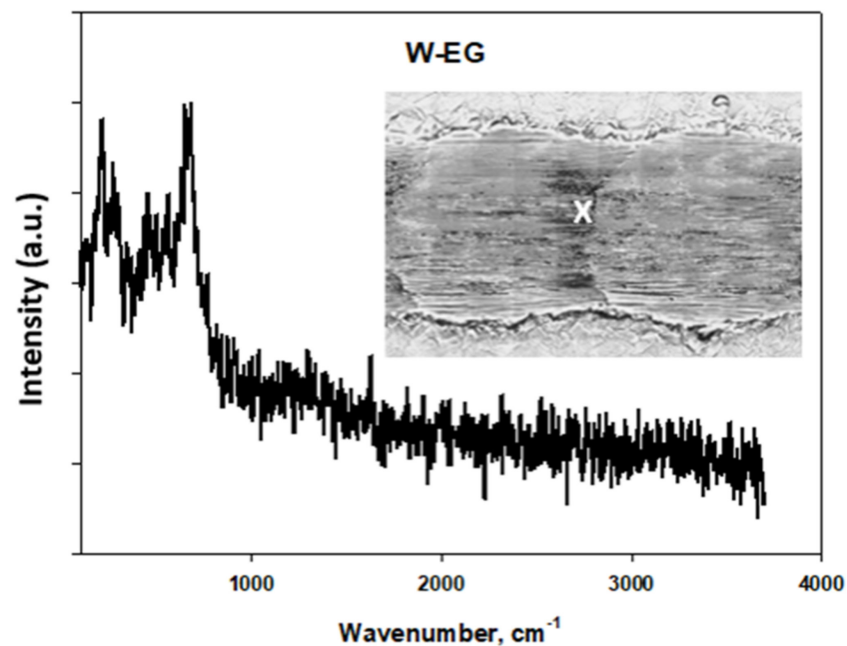
Figure 13. Raman spectrum of the selected point (marked with a white X) inside the wear track, after lubrication with W–EG.

Figure 14 shows the Raman spectrum corresponding to the marked spot closer to the wear track edge. In this case, the main band is observed at 672.3 cm^{-1}, which can be assigned to Fe$_3$O$_4$ oxide [35,36].
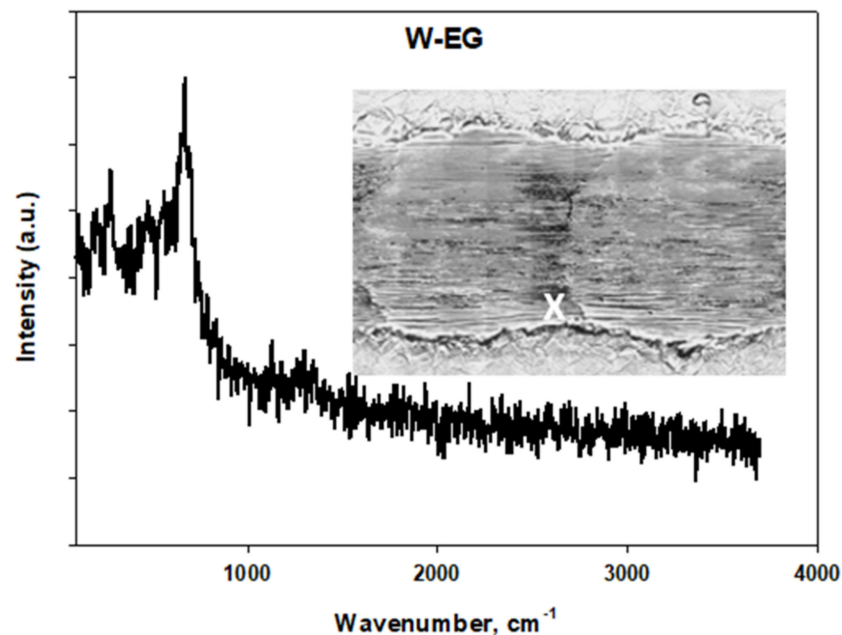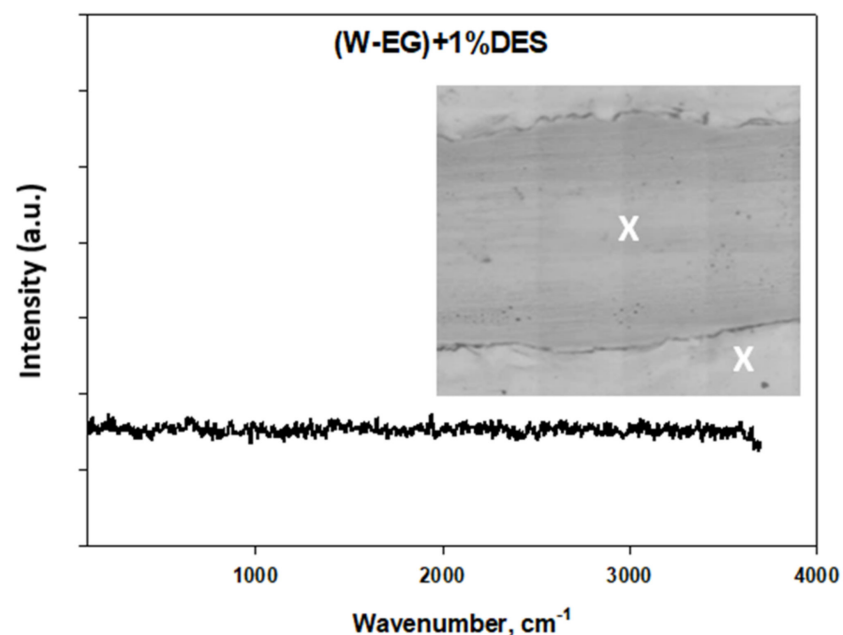

Figure 14. Raman spectrum of the selected point (marked with a white X) near the edge of the wear track, after lubrication with W–EG.

Finally, Figure 15 shows that at the darker, more plastically deformed region of the wear track, the intensities of both bands, at 273.3 and 683.2 cm^{-1}, are similar, showing the presence of both Fe$_2$O$_3$ and Fe$_3$O$_4$ iron oxides.

Figure 15. Raman spectrum of the selected point (marked with a white X) of the dark region inside the wear track shown in the inset, after lubrication with W–EG.

When the new emulsions are used as lubricants, Raman spectra are the same inside and outside the wear path (Figure 16), thus showing the absence of iron oxides. Only at the edge of the wear track (Figure 17), a Raman band at 215.9 cm^{-1}, assignable to Fe-O stretching, is observed.

Figure 16. Raman spectrum of both selected points (marked with a white X) inside and outside the wear track, after lubrication with (W–EG) + 1%DES.
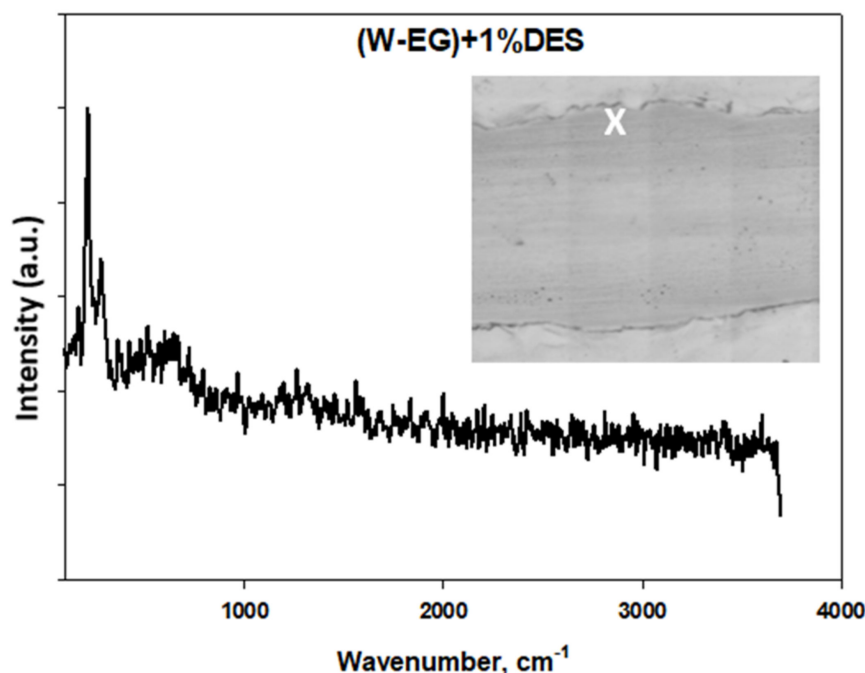
Figure 17. Raman spectrum of the selected point (marked with a white X) inside the wear track after lubrication with (W–EG) + 1%DES.

These results show that the addition of DES not only reduces friction and wear, but also prevents severe oxidation processes.

4. Conclusions

New lubricants have been prepared by adding variable concentrations of the fatty acid-derived protic ionic liquid bis(2-hydroxyethyl)ammonium stearate to water-ethylene glycol (50:50). The new lubricants show similar thermal stability to water-ethylene glycol solution.

While water-ethylene glycol is a Newtonian fluid, the emulsions show a shear thinning effect. Viscosity and turbidity values of the emulsions are higher than those of the water-ethylene glycol solution and increase with increasing protic ionic liquid content. Under variable temperature, reductions in turbidity and viscosity values observed for the emulsions, particularly for that with the highest protic ionic liquid concentration, are related to transitions of the protic ionic liquid additive to the liquid crystal and isotropic liquid states.

The addition of the protic ionic liquid crystal increases contact angles on the stainless steel surface. The tribological performance of the water-ethylene glycol solution is very poor, with a friction coefficient of 0.28 and a wear rate of the order of 1.92×10^{-5} mm^3/N·m. The best friction reduction and antiwear results, with friction and wear reductions of up to 76% and 80%, respectively, are achieved for the emulsions with the lowest viscosity and turbidity values.

The surface damage after lubrication with water-ethylene glycol is very severe, both on the steel and sapphire surfaces. The plastic deformation of the steel is combined with a severe abrasion mechanism that produces parallel grooves inside the wear track. The addition of 0.5 wt.% protic ionic liquid reduces plastic deformation and prevents abrasion. Mild abrasive wear appears again for 1 wt.% and, especially, for 2 wt.% protic ionic liquid proportions.

Surface analyses by EDX show that, after lubrication with water-ethylene glycol, the content of oxygen increases inside the wear track, on the steel surface. Raman microscopy shows the presence of iron oxides such as Fe_2O_3 and Fe_3O_4 inside the wear track surface.

In contrast, lubricants containing the protic ammonium stearate additive reduce or inhibit this oxidation process.

The results described here confirm that water-glycol systems modified by low toxicity, biodegradable protic ionic liquids can combine a good tribological performance with a corrosion protection effect.

References

1. Tomala, A.; Karpinska, A.; Werner, W.S.M.; Olver, A.; Störi, H. Tribological properties of additives for water-based lubricants. *Wear* **2010**, *269*, 804–810. [CrossRef]
2. Igari, S.; Mori, S.; Takikawa, Y. Effects of molecular structure of aliphatic diols and polyalkylene glycol as lubricants on the wear of aluminum. *Wear* **2000**, *244*, 180–184. [CrossRef]
3. Wang, H.; Liu, Y.; Liu, W.; Liu, Y.; Wang, K.; Li, J.; Ma, T.; Eryilmaz, O.L.; Shi, Y.; Erdemir, A. Superlubricity of polyalkylene glycol aqueous solutions enabled by ultrathin layered double hydroxide nanosheets. *ACS Appl. Mater. Interfaces* **2019**, *11*, 20249–20256. [CrossRef] [PubMed]
4. Li, J.; Zhang, C.; Deng, M.; Luo, J. Reduction of friction stress of ethylene glycol by attached hydrogen ions. *Sci. Rep.* **2014**, *4*, 7226. [CrossRef]
5. Lu, X.H.; Yao, K.W.; Ouyang, J.; Tian, Y. Tribological characteristics and tribo-chemical mechanisms of Al-Mg-Ti-B coatings under water-glycol lubrication. *Wear* **2015**, *326*, 68–73. [CrossRef]
6. Singh, T.; Jain, M.; Ganguli, D.; Ravi, K. Evaluation of water glycol hydraulic fluids: A tribological approach. *J. Synthetic Lubrication* **2006**, *23*, 177–184. [CrossRef]
7. Kumar, B.; Singh, T.; Rao, K.S.; Pal, A.; Kumar, A. Thermodynamic and spectroscopic studies on binary mixtures of imidazolium ionic liquids in ethylene glycol. *J. Chem. Thermodyn.* **2008**, *40*, 32–39. [CrossRef]
8. Singh, T.; Kumar, A. Volumetric behaviour of 1-butyl-3-methyl imidazolium hexafluorophosphate with ethylene glycol derivatives: Application of Prigogine-Flory-Patterson theory. *J. Mol. Liq.* **2010**, *153*, 117–123. [CrossRef]
9. Pal, A.; Gaba, R.; Singh, T.; Kumar, A. Excess thermodynamic properties of binary mixtures of ionic liquid (1-butyl-3-methylimidazolium hexafluorophosphate) with alkoxyalkanols at several temperatures. *J. Mol. Liq.* **2010**, *154*, 41–46. [CrossRef]
10. Somers, A.E.; Howlett, P.C.; MacFarlane, D.R.; Forsyth, M. A Review of Ionic Liquid Lubricants. *Lubricants* **2013**, *1*, 3–21. [CrossRef]
11. Zhou, Y.; Qu, J. Ionic liquids as lubricant additives: A review. *ACS Appl. Mater. Interfaces* **2017**, *9*, 3209–3222. [CrossRef]
12. Zhao, S.; Yan, L.; Cao, M.; Huang, L.; Yang, K.; Wu, S.; Lan, M.; Niu, G.; Zhang, W. Near-infrared light-triggered lysosome-targetable carbon dots for photothermal therapy of cancer. *ACS Appl. Mater. Interfaces* **2021**, *13*, 53610–53617. [CrossRef]
13. Greaves, T.L.; Drummond, C.J. Protic ionic liquids: Evolving structure–property relationships and expanding applications. *Chem. Rev.* **2015**, *115*, 11379–11448. [CrossRef]
14. Jordan, A.; Gathergood, N. Biodegradation of ionic liquids—A critical review. *Chem. Soc. Rev.* **2015**, *44*, 8200–8237. [CrossRef]
15. Santos, D.; Costa, F.; Franceschi, E.; Santos, A.; Dariva, C.; Mattedi, S. Synthesis and physico-chemical properties of two protic ionic liquids based on stearate anion. *Fluid Phase Equilibria* **2014**, *376*, 132–140. [CrossRef]
16. Rahman, M.H.; Warneke, H.; Webbert, H.; Rodriguez, J.; Austin, E.; Tokunaga, K.; Rajak, D.K.; Menezes, P.L. Water-Based Lubricants: Development, Properties, and Performances. *Lubricants* **2021**, *9*, 73. [CrossRef]
17. Del Sol, I.; Gamez, A.J.; Rivero, A.; Iglesias, P. Tribological performance of ionic liquids as additives of water-based cutting fluids. *Wear* **2019**, *426*, 845–852. [CrossRef]
18. Sagraloff, N.; Dobler, A.; Tobie, T.; Stahl, K.; Ostrowski, J. Development of an oil-free water-based lubricant for gear applications. *Lubricants* **2019**, *7*, 33. [CrossRef]

19. Khanmohammadi, H.; Wijanarko, W.; Espallargas, N. Ionic liquids as additives in water-based lubricants: From surface adsorption to tribofilm formation. *Tribol. Lett.* **2020**, *68*, 130. [CrossRef]

20. Dong, R.; Yu, Q.; Bai, Y.; Ma, Z.; Zhang, J.; Zhang, C.; Yu, B.; Zhou, F.; Liu, W.; Cai, M. Towards superior lubricity and anticorrosion performances of proton-type ionic liquids additives for water-based lubricating fluids. *Chem. Eng. J.* **2020**, *383*, 123201. [CrossRef]

21. Espinosa, T.; Jiménez, M.; Sanes, J.; Jimenez, A.E.; Iglesias, M.; Bermudez, M.D. Ultralow friction with a protic ionic liquid boundary film at the water-lubricated sapphire-stainless steel interface. *Tribol. Lett.* **2014**, *53*, 1–9. [CrossRef]

22. Avilés, M.D.; Carrión, F.J.; Sanes, J.; Bermúdez, M.D. Bio-based ionic liquid crystal for stainless steel-sapphire high temperature ultralow friction. *Wear* **2021**, *485*, 204020. [CrossRef]

23. Avilés, M.D.; Pamies, R.; Sanes, J.; Arias-Pardilla, J.; Carrión, F.J.; Bermúdez, M.D. Protic ammonium bio-based ionic liquid crystal lubricants. *Tribol. Int.* **2021**, *158*, 106917. [CrossRef]

24. Avilés, M.D.; Cao, V.D.; Sánchez, C.; Arias-Pardilla, J.; Carrión-Vilches, F.J.; Sanes, J.; Kjøniksen, A.L.; Bermúdez, M.D.; Pamies, R. Effect of temperature on the rheological behavior of a new aqueous liquid crystal bio-lubricant. *J. Mol. Liquids* **2020**, *301*, 112406. [CrossRef]

25. Su, T.; Song, G.; Zheng, D.; Ju, C.; Zhao, Q. Facile synthesis of protic ionic liquids hybrid for improving antiwear and anticorrosion properties of water-glycol. *Tribol. Int.* **2021**, *153*, 106660. [CrossRef]

26. Zheng, D.; Su, T.; Ju, C. Influence of ecofriendly protic ionic liquids on the corrosion and lubricating properties of water-glycol. *Tribol. Int.* **2022**, *165*, 107283. [CrossRef]

27. Avilés, M.D.; Carrión, F.J.; Sanes, J.; Bermúdez, M.D. Effects of protic ionic liquid crystal additives on the water-lubricated sliding wear and friction of sapphire against stainless steel. *Wear* **2018**, *408–409*, 56–64. [CrossRef]

28. Avilés, M.D.; Pamies, R.; Sanes, J.; Carrión, F.J.; Bermúdez, M.D. Fatty acid-derived ionic liquid lubricant. Protic ionic liquid crystal as additive of protic ionic liquid. *Coatings* **2019**, *9*, 710. [CrossRef]

29. Wang, Y.R.; Yu, Q.L.; Cai, M.R.; Shi, L.; Zhou, F.; Liu, W.M. Ibuprofen-based ionic liquids as additives for enhancing the lubricity and antiwear of water-ethylene glycol liquid. *Tribol. Lett.* **2017**, *65*, 13. [CrossRef]

30. Zheng, G.; Zhang, T.; Ding, X.; Xiang, F.; Li, T.; Lui, S.; Zheng, L. Tribological properties and surface interaction of novel water-soluble ionic liquid in water-glycol. *Tribol. Int.* **2017**, *116*, 440–448. [CrossRef]

31. Krishan, K.; Krishan, R.S. Raman and infrared spectra of ethylene glycol. *Proc. Indian Acad. Sci. A* **1988**, *64*, 111. [CrossRef]

32. Binnemans, K. Ionic Liquid Crystals. *Chem. Rev.* **2006**, *105*, 4148–4204. [CrossRef]

33. Maximo, G.J.; Santos, R.J.B.N.; Lopes-da-Silva, J.A.; Costa, M.C.; Meirelles, A.J.A.; Coutinho, J.A.P. Lipidic Protic Ionic Liquid Crystals. *ACS Sustain. Chem. Eng.* **2014**, *2*, 672–682. [CrossRef]

34. Maleki, A.; Zhu, K.; Pamies, R.; Rodríguez-Schmidt, R.; Kjøniksen, A.L.; Karlsson, G.; Hernández-Cifre, J.G.; García de la Torre, J.; Nyström, B. Effect of polyethylene glycol (PEG) length on the association properties of temperature-sensitive amphiphilic triblock copolymers (PNIPAAMm-b-PEGn-b-PNIPAAMm) in aqueous solution. *Soft Matter* **2011**, *7*, 8111–8119. [CrossRef]

35. Ramya, S.; Anita, T.; Shaikh, H.; Dayal, R.K. Laser Raman microscopic studies of passive films formed on type 316LN stainless steels during pitting in chloride solution. *Corrosion Sci.* **2010**, *52*, 2114–2121. [CrossRef]

36. Cui, Y.; Shuming, L.; Smith, K.; Kanghua, Y.; Hongying, H.; Jiang, W.; Li, Y. Characterization of corrosion scale formed on stainless steel delivery pipe for reclaimed water treatment. *Water Res.* **2016**, *88*, 816–825. [CrossRef]